nature geoscience

LETTERS

PUBLISHED ONLINE: 8 DECEMBER 2013 | DOI: 10.1038/NGEO2025

Evidence for biogenic graphite in early Archaean Isua metasedimentary rocks

Yoko Ohtomo[1]*, Takeshi Kakegawa[1], Akizumi Ishida[1], Toshiro Nagase[1] and Minik T. Rosing[2]

Some graphite contained in the 3.7-billion-year-old metasedimentary rocks of the Isua Supracrustal Belt, Western Greenland[1], is depleted in ^{13}C and has been interpreted as evidence for early life[2]. However, it is unclear whether this graphite is primary, or was precipitated from metamorphic or igneous fluids[3,4]. Here we analyse the geochemistry and structure of the ^{13}C- depleted graphite in the Isua schists. Raman spectroscopy and geochemical analyses indicate that the schists are formed from clastic marine sediments that contained ^{13}C-depleted carbon at the time of their deposition. Transmission electron microscope observations show that graphite in the schist occurs as nanoscale polygonal and tube-like grains, in contrast to abiotic graphite in carbonate veins that exhibits a flaky morphology. Furthermore, the graphite grains in the schist contain distorted crystal structures and disordered stacking of sheets of graphene. The observed morphologies are consistent with pyrolysation and pressurization of structurally heterogeneous organic compounds during metamorphism. We thus conclude that the graphite contained in the Isua metasediments represents traces of early life that flourished in the oceans at least 3.7 billion years ago.

The suggestion that graphite in early Archaean rocks represents materials of biogenic origin has been met with a degree of scepticism[5,6]. Isotopic compositions of graphite in >3.7-billion-year old (Ga) rocks from the Isua Supracrustal Belt (ISB), Western Greenland, which are believed to be of sedimentary origin, suggest that vast microbial ecosystems were present in early Archaean oceans[7,8]. However, results of more recent studies suggest that most of the graphite-bearing rocks formed through interactions between crustal fluids and surrounding igneous rocks[3,4] during later metasomatic events[9], thereby casting doubt on the existence of an extensive sedimentary sequence in the ISB and on the biogenic origin of constituents. In contrast, ^{13}C-depleted graphite globules, which are considered to form from biogenic precursors, have been reported from metamorphosed clastic sedimentary rocks in the ISB (ref. 2). However, these globules were found at a single locality, and it therefore remains unclear whether traces of life at other localities in the ISB were lost during metamorphism or were originally absent. The presence of additional clastic sedimentary rocks containing graphite may provide evidence for the preservation of organic constituents in early Archaean rocks, thus supporting the notion that microbes were active in early Archaean oceans.

We conducted a geological survey along the northwestern area of the ISB (Fig. 1a,b), where the rocks are generally less affected by deformation than in other areas of the belt[10]. Metamorphosed basalts and banded iron formations (BIFs) are dominant in this area. The BIFs contain interbedded black to grey schist layers (Fig. 1b–d), typically 40–80 cm thick. The schist mainly comprises chlorite, cummingtonite, quartz and reduced carbon (see Supplementary Fig. 1 and Table 1). The black–grey schist in the northern part of the area contains moderate amounts of Al, Ti and Zr, probably representing detrital components (see Supplementary Information). The rare earth element (REE) patterns (normalized by the composition of post-Archaean Australian shale, PAAS; ref. 11) in the Al-rich rocks (samples 3072303 and 6072905) lie close to the line defined by a rock/PAAS ratio of 1, with the exception of slightly lower ratios for light REEs (Fig. 2). These REE patterns and Al-rich characteristics suggest that the protoliths of the schist were clastic marine sediments. However, some of the examined rocks have compositions resembling those of BIFs (for example, samples 4062308, 4062309 and 5080501).

The black–grey schist samples contain abundant reduced carbon (0.1–8.8 wt%), identified as graphite by X-ray diffraction (XRD) analysis (Supplementary Tables 3 and 4). The graphite-rich schist from the northern part of the area is folded, as are the surrounding BIFs. A sample from this folded area contains the highest concentrations of $C_{graphite}$ (8.8 wt% C) measured in the present study. At other locations, the schist is concordantly intercalated in layers of BIFs, and contains moderate concentrations of $C_{graphite}$ (0.1–0.5 wt% C; Supplementary Table 3). In general, graphite concentrations on microscopic scales vary according to the compositional layering of the schist, which strikes parallel to that of the surrounding BIFs. Thus, the moderate to high $C_{graphite}$ concentrations, the correspondence of $C_{graphite}$ concentrations with compositional layering and the concordant layering of schist and BIF units all support a sedimentary origin of the reduced carbon.

It has been suggested that disproportionation of Fe-carbonate during metamorphism accounts for the genesis of the graphite in secondary carbonate veins[4]. In such veins, substantial amounts of magnetite and residual Fe-carbonate occur along with the graphite. However, Fe-carbonate and magnetite are absent from the graphite-rich schist in this study. Therefore, it is unlikely that the graphite originated from the thermal disproportionation of Fe-carbonate.

A graphite-rich carbonate vein, located in the northeastern part of the ISB, contains high concentrations of graphite (sample 4062002y, 4.1 wt% C; see Supplementary Table 3) compared with other carbonate veins in the ISB, which contain much smaller amounts of graphite if any (see Supplementary Information). Such secondary graphite was analysed together with graphite in the metasediment. The geothermometric signals of the Raman spectrum in metasediment sample 6072905 indicate that peak metamorphic temperatures of the graphite were 525 ± 50 °C, which is consistent with prograde metamorphic temperatures reported for the ISB (500–600 °C; ref. 9). This temperature consistency

[1]Natural Resources and Environmental Geochemistry Research Group, Division of Earth and Planetary Materials Science, Graduate School of Science, Tohoku University, 980-8578, Japan, [2]Nordic Center for Earth Evolution, Natural History Museum of Denmark, University of Copenhagen, 1350, Denmark. *e-mail: ohtomoy@jamstec.go.jp

© 2013 Macmillan Publishers Limited. All rights reserved.

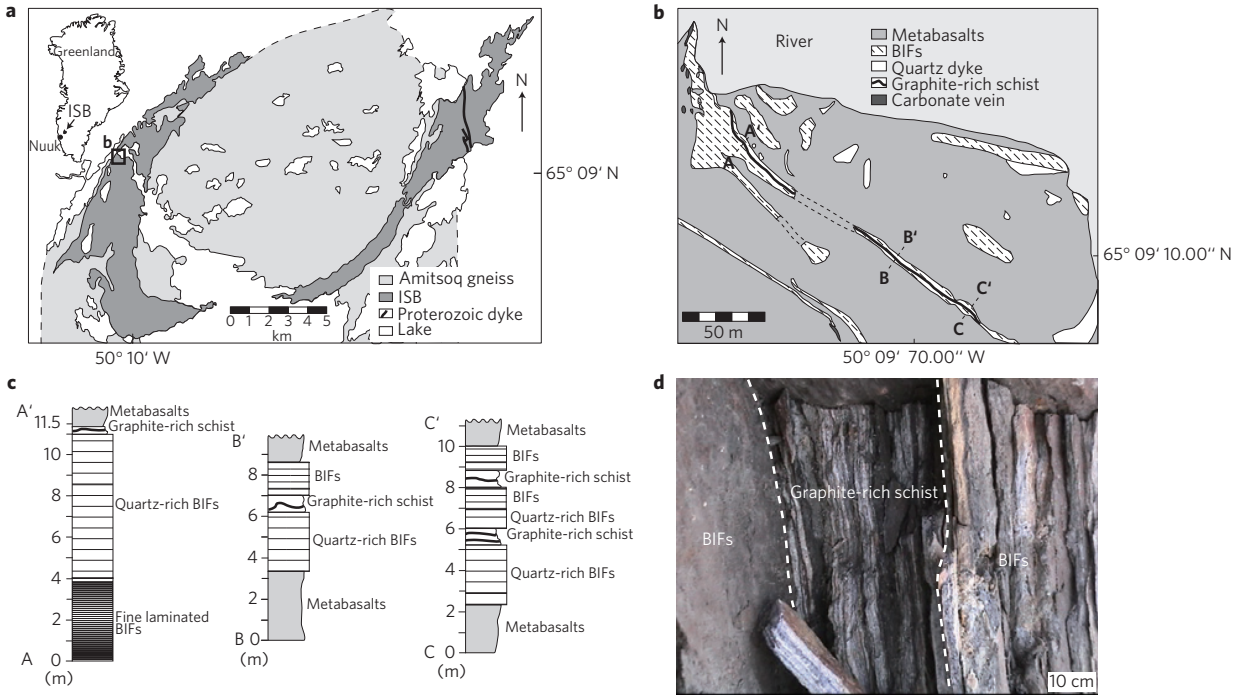

Figure 1 | Geologic maps and photos of the study area in the ISB, West Greenland. a, General geology of the ISB, West Greenland. **b**, Geologic map produced in this study. **c**, Geologic cross-sections A–A′ (northern section), B–B′ (central section) and C–C′ (southern section). Points along A–C′ are the same as those presented in **b**. **d**, Outcrop photograph of graphite-rich schist intercalated with BIFs.

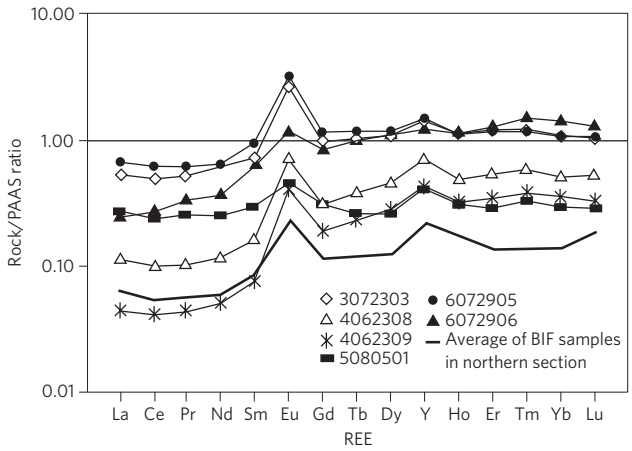

Figure 2 | REE patterns in the examined graphite-rich schist. The BIF value in this figure represents the average composition of nine BIF samples from along the northern section A–A′ (Fig. 1b).

suggests that the precursor of the graphite was already present in the host rocks before prograde metamorphism. Raman spectrum of secondary graphite (sample 4062002y) is nearly identical to that of the graphite in the metasediment. The estimated metamorphic temperatures for the secondary graphite ($496 \pm 50\,^{\circ}C$) are close to peak metamorphic temperatures, suggesting a metamorphic origin of the secondary graphite.

The carbon isotope ratios ($\delta^{13}C$) of graphite were determined using the graphite combustion method and the neodymium–yttrium aluminium garnet (Nd–YAG) laser microprobe technique. The range of $\delta^{13}C$ values was −23.8 to −12.5‰ (average, −17.9‰), which is within the range of values reported in previous studies (Fig. 3). The $\delta^{13}C$ value of the secondary graphite (sample 4062002y) was −10.5‰ (Supplementary Table 3). The Nd–YAG laser microprobe analysis revealed microscale heterogeneities in the $\delta^{13}C$ values in single rock chips ($10 \times 5 \times 0.5\,mm^3$; Fig. 3b,c and Supplementary Fig. 2). For example, the $\delta^{13}C$ values for sample 5080603 ranged from −20.9 to −14.7‰ (average, −17.4‰; Fig. 3c).

Carbonic fluids can precipitate abiogenic graphite during isobaric cooling, during isothermal increases in pressure[12] and on account of the mixing of CH_4- and CO_2-rich fluids[13]. We modelled the theoretical $\delta^{13}C$ values of fluid-precipitated graphites[14], assuming that the $\delta^{13}C$ value for CO_2 in the original metamorphic fluid was −5‰, which is similar to the value observed regionally in carbonate-rich rocks of the ISB (refs 4,7). The lightest $\delta^{13}C$ value for graphite precipitated from such fluids under metamorphic conditions is −16.4‰, which is achieved at 400 °C (Supplementary Fig. 5a). The $\delta^{13}C$ values exceed −16.4‰ when Rayleigh-type isotope fractionation operates in the fluids. Graphite that is depleted in ^{13}C by more than −16.4‰ can form only if the fluid was derived from a source that already contained abundant ^{13}C-depleted CH_4. However, given the possible oxidation state of infiltrating metamorphic fluids, CH_4 was most probably absent in the fluids (see Supplementary Information).

In samples from central to southern sections (B–B′ and C–C′, respectively; Fig. 1), abundances of $C_{graphite}$ were low and $\delta^{13}C$ values were high, suggesting that extensive reactions with metamorphic fluids shifted $\delta^{13}C$ of graphite to higher $\delta^{13}C$ values (for example, −12.5‰; Supplementary Fig. 3). The heterogeneities in $\delta^{13}C$ values (Fig. 3a–c) are explained by exchange of carbon isotopes with transient carbonic fluids. In other words, all $\delta^{13}C$ of graphite were originally lower than those shown in Fig. 3. The more negative isotopic compositions (for example, −23.8‰) represent less modified components and are closer to premetamorphic compositions. Therefore, ^{13}C-depleted organic matter in Isua clastic sediments is postulated as an initial carbon source to explain the less modified carbon isotope compositions.

We observed the morphologies and nanostructures of graphite in the metasediment and secondary graphite using scanning transmission electron microscopy (STEM) and high-resolution

© 2013 Macmillan Publishers Limited. All rights reserved.

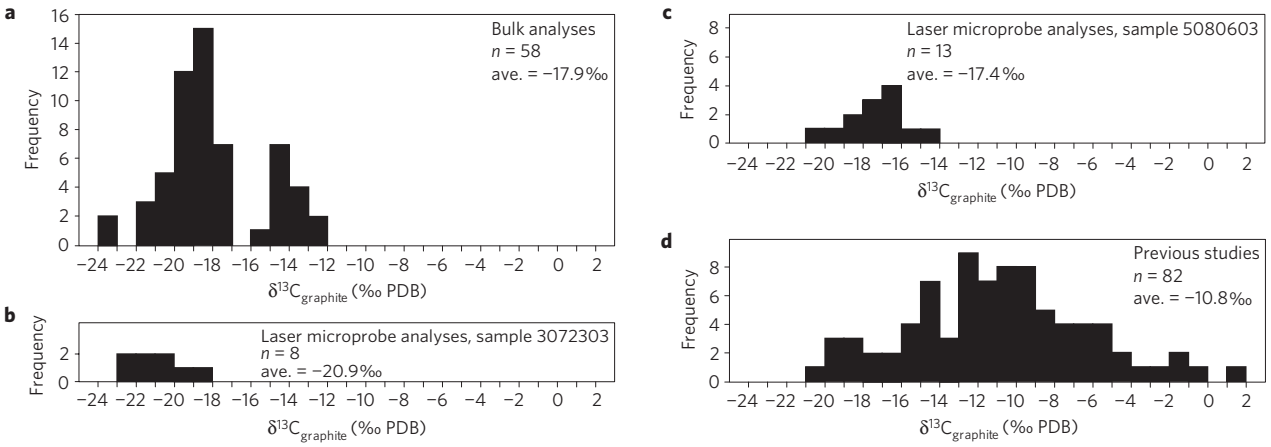

Figure 3 | Carbon stable isotope compositions of graphite in the ISB. a, $\delta^{13}C$ values for graphite in graphite-rich schist extracted from bulk rock powder. **b**, $\delta^{13}C$ values for graphite in sample 3072303 obtained using the Nd-YAG laser microprobe technique. **c**, $\delta^{13}C$ values for graphite in sample 5080603 obtained using the Nd-YAG laser microprobe technique. **d**, Total range of published $\delta^{13}C$ values for graphite in the ISB. Referenced data are listed in Supplementary Table 6. *n*, number of analyses; ave., average value; PDB, Pee Dee Belemnite. Reproducibilities and accuracies of measurements are within ±0.2‰.

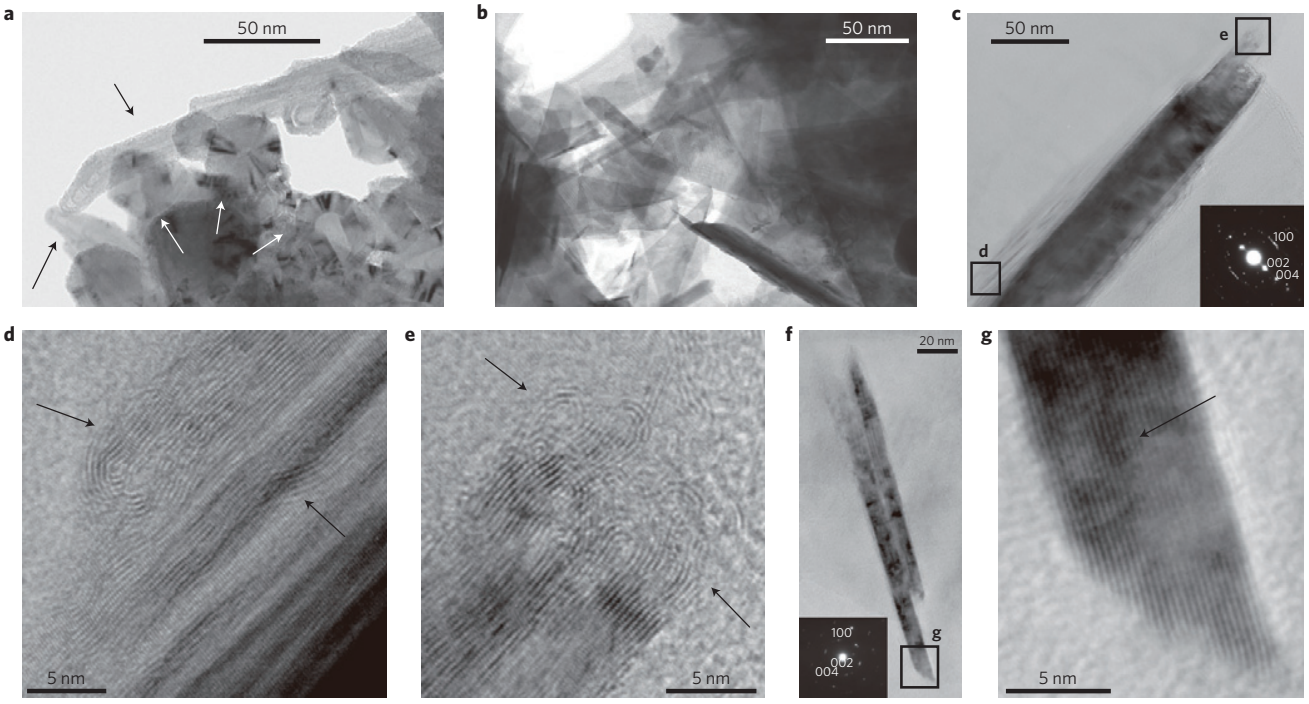

Figure 4 | Transmission electron microscopy images of graphite. a, STEM image of graphite in metasediment (sample 6072906), showing dominance of polygonal and tube-like grains. **b**, STEM image of secondary graphite (sample 4062002y), showing dominance of sheeted flake grains. **c**, HRTEM image of graphite in metasediment (sample 6072905). SAED was obtained from area in **c**. **d**,**e**, Magnification of the area marked **d** and **e** in **c**. **f**, HRTEM image of sample 4062002y. SAED was obtained from area in **f**. **g**, Magnification of the area marked **g** in **f**. Arrows are explained in the main text.

transmission electron microscopy (HRTEM). Irrespective of the sample type, all examined graphite showed highly crystalline features in HRTEM observations, which is consistent with the XRD and Raman data. Differences between graphite in the metasediment and that in the secondary vein samples are reflected in their respective morphologies, internal graphite nanostructures and stacking defects. The examined metasediment included graphitic polygonal grains (white arrows, Fig. 4a) and tube-like structure (black arrows, Fig. 4a). Some lattice fringes showed distortion at surfaces and inside graphite grains (onion-like structures; black arrows, Fig. 4d,e; see Supplementary Information for details). Such features were found in samples from both the northern and southern sections (Supplementary Fig. 9a,b). Sheeted flakes were a dominant morphology of secondary graphite, whereas polygonal grains and tube-like structures were absent (Fig. 4b). The sheeted flakes indicate well-layered structures overall (Fig. 4f,g), although the surfaces and edges of flakes were sometimes curled. Such curled structures disappear on the inner portions of sheeted flakes (black arrow, Fig. 4g; white arrows, Supplementary Fig. 8d,e). The structural changes from the surface to the inner portions of the sheeted flakes indicate that initial deposition of distorted graphite (on the current surface) was followed by ordered deposition of successive layers of graphite (current inner part)[15].

© 2013 Macmillan Publishers Limited. All rights reserved.

In contrast, curled structures are present in the inner portions of graphite grains in the metasediment (black arrows, Fig. 4d), suggesting that its origin is different from that of the secondary graphite. The selected area electron diffraction (SAED) pattern of graphite in the metasediment has ⟨001⟩* streaks on and near the *h*00 reflections (see the bright diffusion line near the 100 plane in the SAED data, Fig. 4c), caused by a disordered stacking sequence of the graphene sheets. However, ⟨001⟩* streaks are unclear in the SAED pattern of Fig. 4f, suggesting a dominance of ordered 2H-type stacking in the secondary graphite.

The effects of temperature, pressure and mineral surfaces on the graphitization of biogenic organic compounds in geological samples have been intensively studied[16–22]. Distorted structures and the diffusion of graphene sheet stacking are common in pyrolysed and pressurized organic compounds. Such precursors commonly contain non-graphitizing carbon, such as non-planar carbon ring compounds associated with abundant pores[16]. At high pressures, organic matter in the presence of various hydrocarbons mixed with non-graphitizing carbon is forced into parallelism, thereby facilitating the formation of hexagonal graphene sheets, whereas the crystal lattice remains distorted and the graphene sheet stacking may display diffusion in SAED patterns. Therefore, biogenic organic matter, which contains various molecules and functional groups, is favoured as the precursor of the graphite observed in the metasediment.

Onion-like carbonaceous materials have also been observed in meteorites[23]. Some onion-like carbonaceous materials in meteorites were formed at >1,000 °C (ref. 23), which exceeds general metamorphic temperatures. Furthermore, graphite in the examined schist has sedimentary characteristics with various morphologies, suggesting that meteoritic origin is unlikely for the Isua graphite. Polygonal and tube-like structures in graphite-rich schist show similarities to those found in artificial nanocarbons formed under evaporation–condensation conditions and in electric discharge systems[15,24]. However, unusual temperature conditions and chemistry of carbon sources to generate artificial nanocarbons are difficult to realize in the Earth's crust. Therefore, we conclude that polygonal and tube-like structures in the graphite-rich schist were generated during maturation processes of organic matter. A minor portion of heterogeneity in the graphitic structural order could be caused by the secondary effects of surrounding minerals[22] and/or dynamic fluid flow processes[15] during metamorphism.

Graphite in the metasediment from the northwest ISB is distinct from the graphite in vein samples. The combined information on geological occurrences, graphite morphologies, nanoscale structures and isotopic compositions of the graphite in the metasediment suggests a biogenic origin. High concentrations of ^{13}C-depleted graphite in these rocks would require widespread biological activity to support the high rate of production and sedimentary delivery of organic matter to the >3.7 Ga ocean floor.

Received 1 May 2013; accepted 5 November 2013;
published online 8 December 2013

References

1. Nutman, A. P., Friend, C. R. L. & Paxton, S. Detrital zircon sedimentary provenance ages for the Eoarchaean Isua supracrustal belt southern West Greenland: Juxtaposition of an imbricated ca. 3700 Ma juvenile arc against an older complex with 3920–3760 Ma components. *Precambrian Res.* **172,** 212–233 (2009).
2. Rosing, M. T. ^{13}C-depleted carbon microparticles in >3700-Ma sea-floor sedimentary rocks from west Greenland. *Science* **283,** 674–676 (1999).
3. Naraoka, H., Ohtake, M., Maruyama, S. & Ohmoto, H. Non-biogenic graphite in 3.8-Ga metamorphic rocks from the Isua district, Greenland. *Chem. Geol.* **133,** 251–260 (1996).
4. Van Zuilen, M., Lepland, A. & Arrhenius, G. Reassessing the evidence for the earliest traces of life. *Nature* **418,** 627–630 (2002).
5. Mojzsis, S. J. *et al.* Evidence for life on Earth before 3,800 million years ago. *Nature* **384,** 55–59 (1996).
6. Fedo, C. M. & Whitehouse, M. J. Metasomatic origin of quartz–pyroxene rock, Akilia, Greenland, and implications for Earth's earliest life. *Science* **296,** 1448–1452 (2002).
7. Schidlowski, M., Appel, P. W. U., Eichmann, R. & Junge, C. E. Carbon isotope geochemistry of the 3.7×10^9-yr-old Isua sediments, West Greenland: Implications for the Archaean carbon and oxygen cycles. *Geochim. Cosmochim. Acta* **43,** 189–199 (1979).
8. Ueno, Y., Yurimoto, H., Yoshioka, H., Komiya, T. & Maruyama, S. Ion microprobe analysis of graphite from ca. 3.8 Ga metasediments, Isua supracrustal belt, West Greenland: Relationship between metamorphism and carbon isotopic composition. *Geochim. Cosmochim. Acta* **66,** 1257–1268 (2002).
9. Rose, N. M., Rosing, M. T. & Bridgwater, D. The origin of metacarbonate rocks in the Archaean Isua supracrustal belt, West Greenland. *Am. J. Sci.* **96,** 1004–1044 (1996).
10. Rosing, M. T., Rose, N. M., Bridgwater, D. & Thomsen, H. S. Earliest part of Earth's stratigraphic record: A reappraisal of the >3.7 Ga Isua (Greenland) supracrustal sequence. *Geology* **24,** 43–46 (1996).
11. Taylor, S. R. & McLennan, S. M. *The Continental Crust: Its Composition and Evolution* (Blackwell, 1985).
12. Luque, F. J. & Rodas, M. Constraints on graphite crystallinity in some Spanish fluid-deposited occurrences from different geologic settings. *Miner. Deposita* **34,** 215–219 (1999).
13. Chamberlain, C. P. & Rumble, D. Thermal anomalies in a regional metamorphic terrane: An isotopic study of the role of fluids. *J. Petrol.* **29,** 1215–1232 (1988).
14. Ray, J. S. Carbon isotopic variations in fluid-deposited graphite: Evidence for multicomponent Rayleigh isotopic fractionation. *Int. Geol. Rev.* **51,** 45–57 (2009).
15. Kuznetsov, V. L., Butenko, Y. V., Zaikovskii, V. I. & Chuvilin, A. L. Carbon redistribution processes in nanocarbons. *Carbon* **42,** 1057–1061 (2004).
16. Buseck, P. R. & Bo-Jun, H. Conversion of carbonaceous material to graphite during metamorphism. *Geochim. Cosmochim. Acta* **49,** 2003–2016 (1985).
17. Large, D. J., Christy, A. G. & Fallick, A. E. Poorly crystalline carbonaceous matter in high-grade metasediments—implications for graphitization and metamorphic fluid compositions. *Contrib. Mineral. Petrol.* **116,** 108–116 (1994).
18. Deurbergue, A., Oberlin, A., Oh, J. H. & Rouzaud, J. N. Graphitization of Korean anthracites as studied by transmission electron microscopy and X-ray diffraction. *Int. J. Coal Geol.* **8,** 375–393 (1987).
19. Rouzaud, J. N. & Oberlin, A. Structure, microtexture, and optical properties of anthracene and saccharose-based carbons. *Carbon* **27,** 517–529 (1989).
20. Bustin, R. M., Ross, J. V. & Rouzaud, J. N. Mechanisms of graphite formation from kerogen: Experimental evidence. *Int. J. Coal Geol.* **28,** 1–36 (1995).
21. Beyssac, O. *et al.* Graphitization in a high-pressure, low-temperature metamorphic gradient: A Raman microspectroscopy and HRTEM study. *Contrib. Mineral. Petrol* **143,** 19–31 (2002).
22. Van Zuilen, M. A. *et al.* Mineral-templated growth of natural graphite films. *Geochim. Cosmochim. Acta* **83,** 252–262 (2012).
23. Le Guillou, C. *et al.* High resolution TEM of chondritic carbonaceous matter: Metamorphic evolution and heterogeneity. *Meteorit. Planet. Sci.* **47,** 345–362 (2012).
24. Horváth, Z. E. *et al.* Inexpensive, upscalable nanotube growth methods. *Curr. Appl. Phys.* **6,** 135–140 (2006).

Acknowledgements

We thank E. Aoyagi for technical assistance with STEM and HRTEM observations. The isotope ratio mass spectrometer (infrared-MS) analyses were carried out with support from T. Watanabe and F. W. Nara. The manuscript was improved by discussions with Y. Furukawa and T. Otake. This study was supported by the Japan Society for the Promotion of Science (grants 17403011 and 21403009).

Author contributions

Y.O., T.K. and M.T.R. conducted the geological surveys and collected rock samples. Y.O. carried out the geological and petrographical analyses, carbon stable isotope analyses of graphite using the graphite combustion method, XRD analyses, HRTEM observations and thermodynamic/isotopic calculations. A.I. and T.N. contributed to sample preparation and HRTEM observations. T.K. carried out carbon stable isotope analyses of graphite using the *in situ* Nd–YAG laser microprobe technique, STEM observations and Raman microspectroscopic analyses.

Additional information

Supplementary information is available in the online version of the paper. Reprints and permissions information is available online at www.nature.com/reprints. Correspondence and requests for materials should be addressed to Y.O.

Competing financial interests

The authors declare no competing financial interests.

© 2013 Macmillan Publishers Limited. All rights reserved.